

Kinematic Analysis of Minimum Bias and Hard Probes jet streams at ATLAS-LHC

Lucas Silva^{1,a}

¹Faculdade de Ciências da Universidade de Lisboa, Portugal

Project supervisor: Helena Santos

October 16, 2023

Abstract. This project analysed a heavy nuclei run at ATLAS LHC with data collected via two triggers, one of Minimum Bias, and one of Hard Probes (this one being a stream, which is reconstructed with 3 software releases). This analysis relied on performing different cuts of the resulting jets, on 3 kinematic variables, and on 2 transverse momentum values, and observing the resulting η , ϕ and p_T distributions.

KEYWORDS: LHC, ATLAS, jets, Kinematic analysis

1 Introduction

1.1 The ATLAS experiment and relevant Detectors

The ATLAS experiment is general purpose and characterised by a wealth of sensors, capturing a great amount of data through which high spatial resolution is achieved. It is used to study proton-proton collisions as well as heavy nuclei collisions. In this case it is used for the analysis of lead nuclei impacts, in the 2022 pilot run.

The detectors relevant to this particular case are the Forward Calorimeter and the Inner Detector (constituted by the Pixel Detector, the Semiconductor Detector and the Transition Radiation Detector).

The Forward Calorimeter, which is a part of the Liquid Argon Calorimeter [1] is located perpendicularly to the particles trajectories before collision. It allows the collection of the energy of particles which collide with it, by absorbing the incoming particles in the metal, and registering the current produced in the Argon between its layers. This allows the determination of the Transverse Energy ($FCal_{Et}$) of a jet created.

The Inner Detector (ID) [2], on whose outside lies the Liquid Argon Calorimeter, allows us to determine μ , the visible number of proton-proton (p-p) collisions per visible bunch crossing, as well as NPV (number of primary vertices). These variables, as well as the Transverse Energy are event-level, meaning for every snapshot of a collision (usually consisting of multiple jets), there is one value for each. The innermost part of the ID is the Pixel Detector, which, through the usage of minute pixels which record deposits of energy of passing particles. This works in tandem with the Semiconductor Detector, which has multiple layers of silicon, allowing the building of a track of the particle movement, allowing the determination of how many Primary Vertices of collision occurred. This detector also allows the determination of the μ , measuring the luminosity at the time of collision. Instantaneous luminosity is determined by how particle dense the accelerated beam is [3].

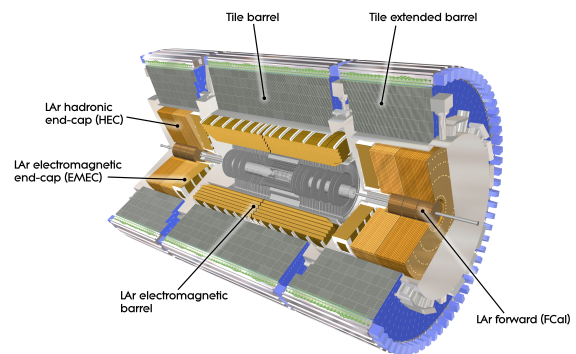


Figure 1: Schematic view of the Calorimeters in ATLAS

1.2 Jets

Jets are clusters of collimated particles resultant from a collision, detected in the Inner Detector as localized energy deposits. They are produced in a hard scattering process, where the initial beams have high transverse momentum (p_T). The borders of jets and how many exist are variables defined using jet construction algorithms, the chosen one in the data analysed being the anti- K_t algorithm. This algorithm produces circular hard jets, being close to cone algorithms while being less complex [4].

Some energy deposits from soft scattering or background noise may also be wrongly constructed as jets in the running algorithm, and these false jets need to be filtered out so that the reconstruction process, which reconstructs partons at the collision from the jets, is as little affected as possible. The jets themselves, and their difference in relation to predictions based on p-p collisions, give information regarding the constitution of a Quark-Gluon Plasma (QGP) formed after the collision of heavy nuclei, which interacts with the jets [5].

The study of the QGP is one of the main motivations for this study of jets and how to filter them efficiently.

The run data is segmented in events, which are snapshots of the collisions occurring, and the jets are analysed per event, along with the event variables, determined by

^ae-mail: fc56415@alunos.fc.ul.pt

the detector readings taking place throughout this snapshot.

1.3 Relevant variables

Here we present a list of the main variables which can be measured with the detector and are used in this analysis.

- θ : polar angle of the trajectory of the particle in relation to the beam axis positive side;
- $\eta = -\ln(\tan \theta/2)$: called pseudorapidity, this is an approximation for high energy particles (for which the mass can be neglected), the original quantity being $\frac{1}{2} \ln \frac{E+p_z}{E-p_z}$;
- ϕ : azimuthal angle of the trajectory of the object in the plane transverse to the direction of the proton beams;
- μ : The average number of visible proton-proton (or Pb-Pb) interactions per bunch crossing per event;
- p_T : transverse momentum, the magnitude of momentum projected in the xy plane - perpendicular to the beam axis;
- NPV : Number of Primary Vertices of collision per event;
- F_{Cal_Et} : Forward Calorimeter transverse energy, measured in an event-by-event basis;

1.4 Analysed data and triggers

The data used in this study is split in two parts. Both elements are from the pilot ion run (Pb+Pb) from 2022, with different triggers, the first file being:

```
user.mrybar.5TeV_HI_2022_MinBias_PVReq_tight_r001.root.
```

This used a Minimum Bias trigger (therefore it will be referred to as MB), defining low thresholds from which collection of events, including soft scattering events along with the desired hard scattering events in the data set. This set was greatly affected by the cuts later imposed, removing low-energy or many-collision events from the sample. The minimum-bias trigger is designed to record a random selection of bunch crossings.

The second set used is composed of 3 software releases of the same run with another trigger, of file names:

```
user.mrybar.data18_hi.00367134.physics_HardProbes_r21_HION7_ANALYSIS.root;
user.mrybar.data18_hi.00367134.physics_HardProbes_r22.0.68_all_EXT0_HIJeTVaI_r002_ANALYSIS.root;
user.mrybar.data18_hi.00367134.physics_HardProbes.merge.AOD.r14821_p5760_rel23_r001_ANALYSIS.root;
```

These used a Hard Probes trigger, defining higher jet p_T thresholds, and thus reducing the amount of soft scattering events. The cuts applied to the Hard Probes data showed greatly diminished results compared to the first set.

1.5 Software used

The analysis and visualization of the data was possible through using Root (<https://root.cern/about/>), and the associated Root TBrowser, running the code for data search, selection and presentation, on the LIP Pauli machines.

2 Analysis procedures

The purpose of the analysis was to determine the effect of event-level variables on the kinematic distribution of jets.

2.1 Variable cuts

To define useful values of each variable presented at which to cut, the histograms of μ , NPV , F_{Cal_Et} - at event level - and p_T - for every jet - for the MB run were analysed.

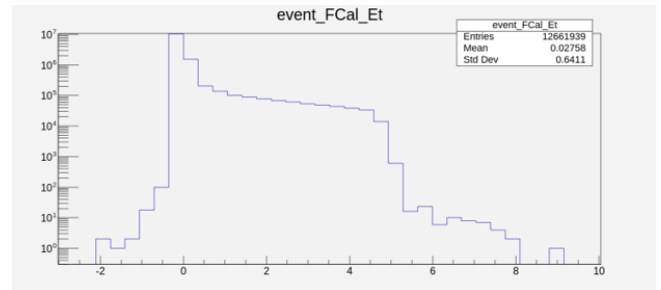


Figure 2: The Forward Calorimeter Transverse Energy distribution (in GeV) of the events registered. Trigger is Minimum Bias

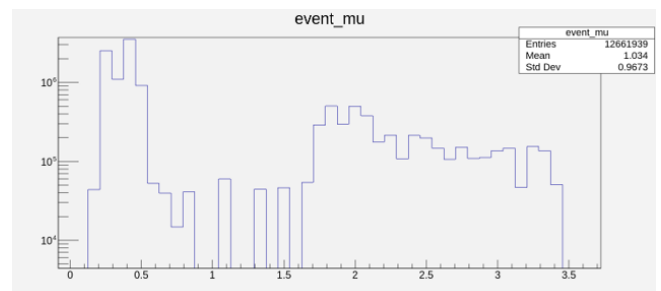


Figure 3: The average number of visible proton-proton (or Pb-Pb) interactions per bunch crossing per event, μ , distribution of the events registered. Trigger is Minimum Bias

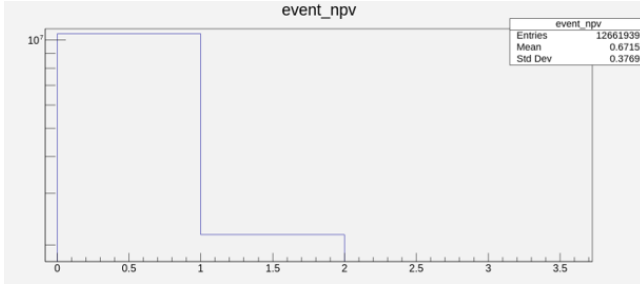


Figure 4: The Number of Primary Vertices, NPV, distribution of the events registered. Trigger is Minimum Bias

As can be seen on the $FCal_Et$ histogram, a cut to remove non-physical events (those with $Et < 0$), removes a significant part of the data, and the decided threshold for such is 0.1 GeV.

On the μ diagram, the chosen threshold is of $\mu < 1$, which also eliminates a large part of the data. This cut owes to the fact that over this limit there is a considerable amount of overlapping information in detectors, hindering analysis and identifying the respective processes. In order to remove uncertainty and promote an easier object reconstruction from the data in the detectors, events with $\mu > 1$ were therefore excluded.

The NPV cut was chosen to prioritize single vertex events, characterized by hard scattering.

As a complementary analysis, the data were also filtered by p_T , with its effect being observed in η and ϕ graphs, there being 3 graphs in comparison - without cut, $p_T > 10$ GeV, $p_T > 30$ GeV.

The cut of 10 GeV was chosen to reduce greatly the effect of the detector's electronic noise, affecting low momentum results. The cut of 30 GeV, on the other hand, was picked to remove partially the effect of the Underlying event (UE). This is caused by soft scattering interactions happening concurrently with the hard scattering of interest, especially in the Pb-Pb collisions whose data are being here analysed, with heavy fluctuations. This source of noise is partly filtered by analysing strips of eta individually, however, in low energy conditions, some information from UE still gets labeled as jets erroneously, which motivates this cut.

2.2 Dividing the jets

In this study, the jets were separated in leading, sub-leading, and inclusive. The leading and sub-leading being defined as the jet in each event which has the highest or second highest transverse momentum attributed, whereas the inclusive analysis used every jet.

3 Data visualization - Kinematic Variable Cuts

3.1 Minimum Bias trigger

3.1.1 p_T graphs

To analyse the p_T distribution of the MB trigger stream, the following three graphs are presented.

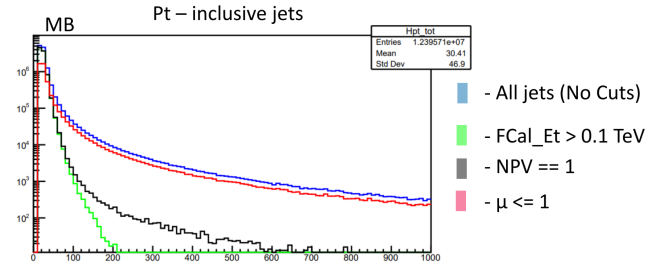


Figure 5: The transverse momentum, p_T , distributions of the inclusive jet sample before and after the respective cuts in legend. Trigger is Minimum Bias.

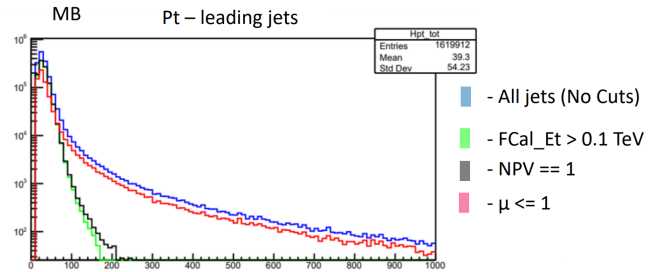


Figure 6: The transverse momentum, p_T , distributions of the leading jet sample before and after the respective cuts in legend. Trigger is Minimum Bias.

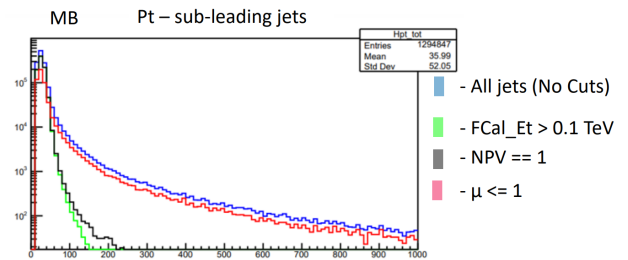


Figure 7: The transverse momentum, p_T , distributions of the sub-leading jet sample before and after the respective cuts in legend. Trigger is Minimum Bias.

It can be seen that in the 3 cases the $FCal_Et$ and the NPV condition are the most impacting in the upper p_T limit, however, due to a greater impact of the μ cut on the lower p_T range, this one ends up removing the most information from the graph. This is an indication of the usefulness of this filter in conjunction with the less selective MB trigger. One can see that the NPV cut is more effective at the upper range in the leading and sub-leading jets than in the inclusive, which does not happen with the Hard Probes trigger stream, as less jets on this p_T range are identified by the algorithm. This prevalence with the MB trigger could be from the capture of events where a

high number of jets (perhaps false, since removed by the cut), have a higher p_T , not just the leading and sub-leading, contributing mostly to the inclusive graph and not to the leading and the sub-leading.

3.1.2 ϕ graphs

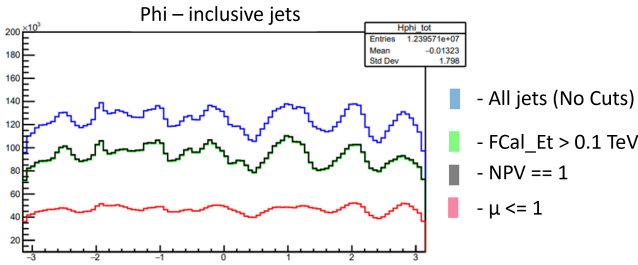


Figure 8: The azimuthal angle, ϕ , distributions of the inclusive jet sample before and after the respective cuts in legend. Trigger is Minimum Bias.

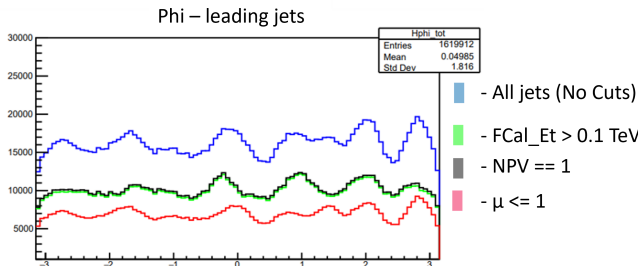


Figure 9: The azimuthal angle, ϕ , distributions of the leading jet sample before and after the respective cuts in legend. Trigger is Minimum Bias.

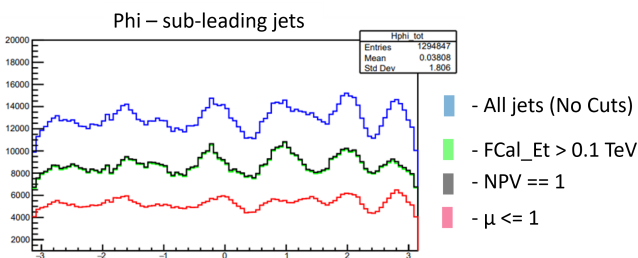


Figure 10: The azimuthal angle, ϕ , distributions of the sub-leading jet sample before and after the respective cuts in legend. Trigger is Minimum Bias.

We observe a distribution of jets fluctuating around the average, originating pronounced spikes. These spikes partially coincide between the leading/sub-leading datasets and the inclusive one, some change being observed in $-2 < \phi < -1$. This spikes may be due to dead elements in the detector itself, interfering with the results in a localized manner. The cuts applied in the inclusive data-set

do not change the angular jet distribution, but on the other 2 sets on the region $1 < \phi < 1.5$, the resulting peak is a sum of those from the NPV and μ cuts, indicating a slight angular difference.

3.1.3 η graphs

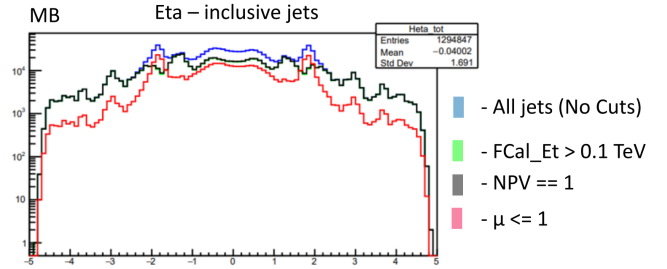


Figure 11: The pseudorapidity, η , distributions of the inclusive jet sample before and after the respective cuts in legend. Trigger is Minimum Bias.

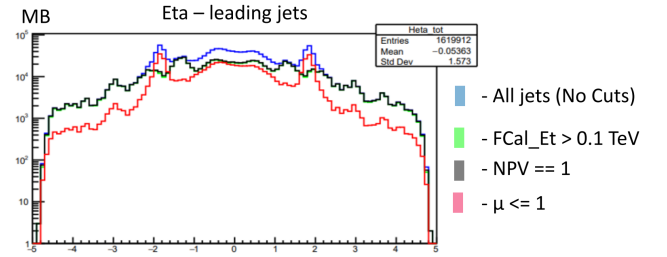


Figure 12: The pseudorapidity, η , distributions of the leading jet sample before and after the respective cuts in legend. Trigger is Minimum Bias.

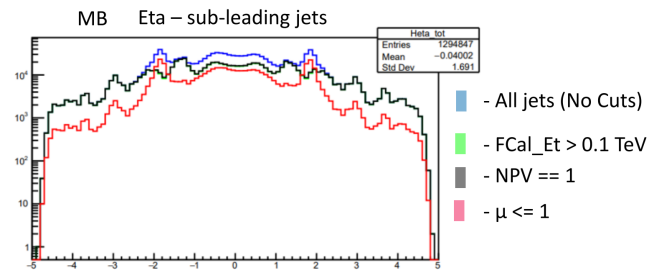


Figure 13: The pseudorapidity, η , distributions of the sub-leading jet sample before and after the respective cuts in legend. Trigger is Minimum Bias.

We can see a symmetry around $\eta = 0$, as expected, and a lateral decline in the three graphs, as well as similar peaks in all sets, attributed to secondary particles that originate in interactions between particles emerging from the primary collisions and the passive material of the detector (that acts as a target). This indicates higher than received energy. Both cuts affect the central portion of lower

η magnitude, but only the μ cut affects the border region, indicating the pervasiveness of higher μ jets, which would be hard to reconstruct to particles, but in the border regions the jets are likely due to hard scattering, since they pass the $NPV = 1$ criterion.

We can see in the preceding MB graphs that the μ cut is the most significant since it cuts significantly lower pT jets, where the pT distribution is denser.

3.2 Hard Probes trigger

3.2.1 p_T graphs - inclusive data-sets

The three software releases were analysed, and will be here presented. Here the only cuts visible are the " $NPV = 1$ " and " $FCal_{Et} > 0.1$ " cuts, though overlapped on the graphs.

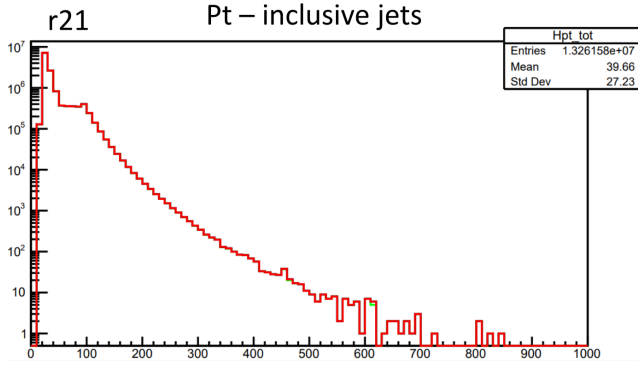


Figure 14: The transverse momentum, p_T , distributions of the inclusive jet sample before and after the respective cuts. Trigger is Hard Probe - r21 release.

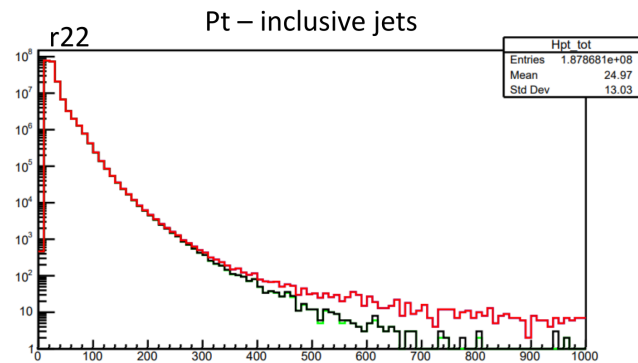


Figure 15: The transverse momentum, p_T , distributions of the inclusive jet sample before and after the respective cuts. Trigger is Hard Probe - r22 release.

It is observed that in the r21 release the cut off point for jets is at a much lower pT value, and the $NPV/FCal_{Et}$ cut does not affect it. For both others this cut approximates this behaviour, indicating that higher pT value jets are originated from multiple collisions events.

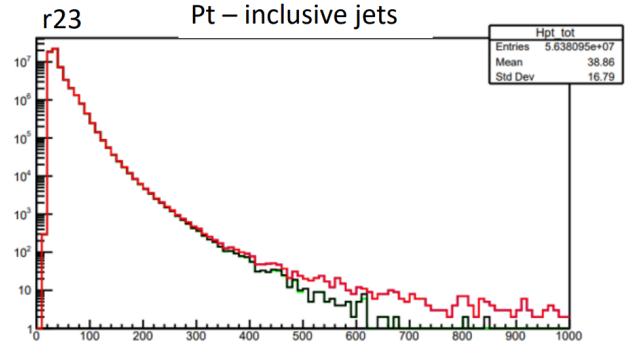


Figure 16: The transverse momentum, p_T , distributions of the inclusive jet sample before and after the respective cuts. Trigger is Hard Probe - r23 release.

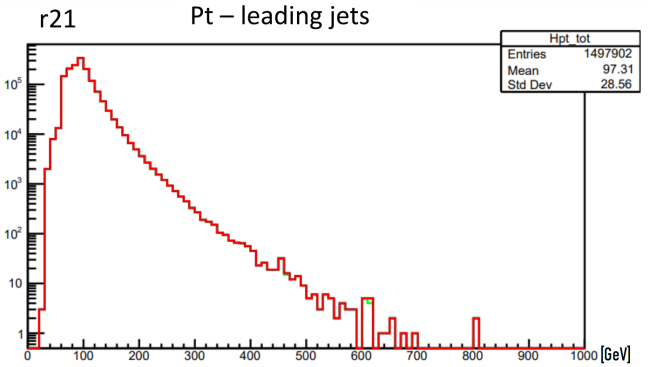


Figure 17: The transverse momentum, p_T , distributions of the leading jet sample before and after the respective cuts. Trigger is Hard Probe - r21 release.

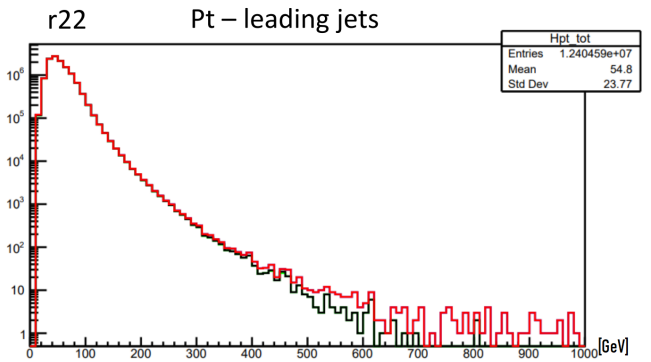


Figure 18: The transverse momentum, p_T , distributions of the leading jet sample before and after the respective cuts. Trigger is Hard Probe - r22 release.

3.2.2 p_T graphs - leading data-sets

It is observed that in the leading set, the initial peak of the pT distribution is at higher pT values, as expected of the jets with the highest pT in each event. The same trend as before is observable regarding the r21 cut off point at lower pT. In this set however, the r21 peak is to the right of the r22 and r23 peaks.

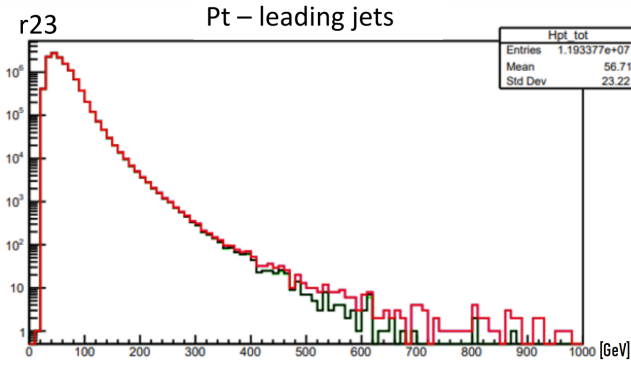


Figure 19: The transverse momentum, p_T , distributions of the leading jet sample before and after the respective cuts. Trigger is Hard Probe - r23 release.

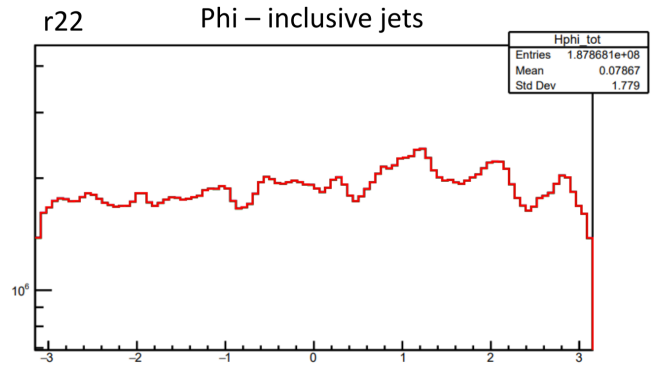


Figure 21: The azimuthal angle, ϕ , distributions of the inclusive jet sample before and after the respective cuts. Trigger is Hard Probe - r22 release.

In both sets it is seen that the r21 release is unaffected by either cut.

No significant difference was observed between the leading and sub-leading graphs of p_T .

3.2.3 ϕ graphs

The variable cuts did not affect either ϕ and η distributions on the Hard Probes releases.

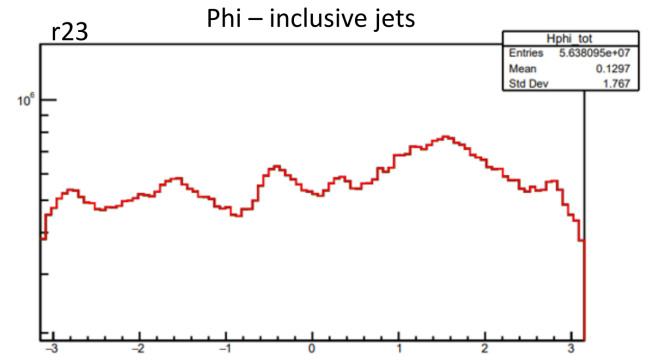


Figure 22: The azimuthal angle, ϕ , distributions of the inclusive jet sample before and after the respective cuts. Trigger is Hard Probe - r23 release.

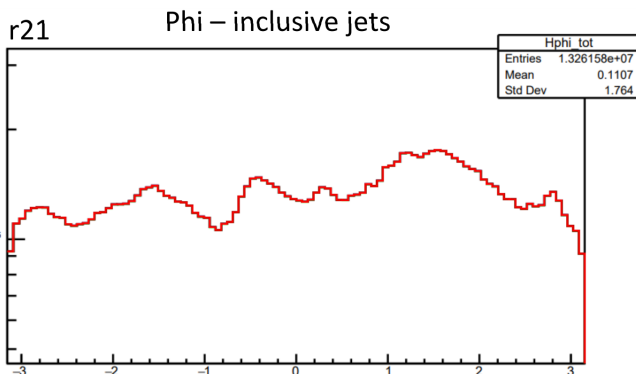


Figure 20: The azimuthal angle, ϕ , distributions of the inclusive jet sample before and after the respective cuts. Trigger is Hard Probe - r21 release.

3.2.4 η graphs - inclusive set

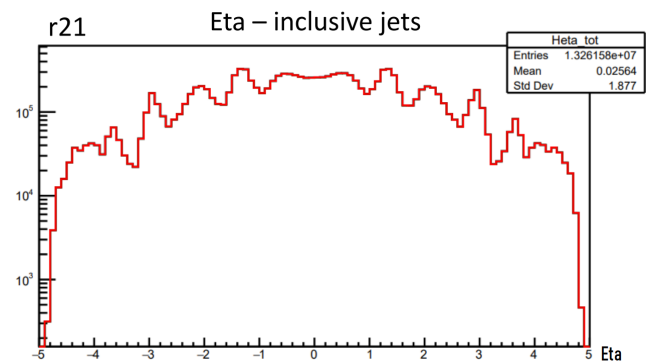


Figure 23: The pseudorapidity, η , distributions of the inclusive jet sample before and after the respective cuts. Trigger is Hard Probe - r21 release.

The r21 and r23 releases match their jet peaks much more closely than with r22, having a peak around $\phi = 1.5$.

The Leading and sub-leading sets showed similar results, with less granularity due to the smaller data-sets.

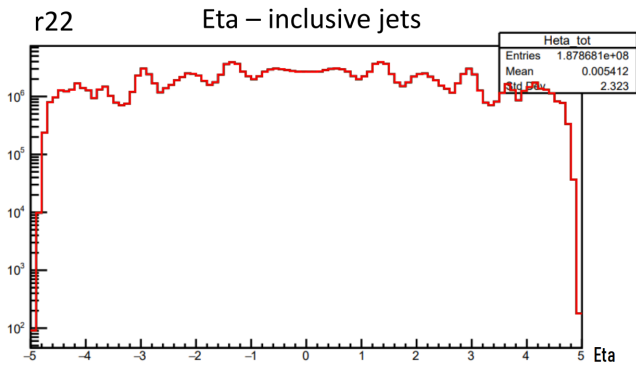


Figure 24: The pseudorapidity, η , distributions of the inclusive jet sample before and after the respective cuts. Trigger is Hard Probe - r22 release.

3.2.5 η graphs - leading set

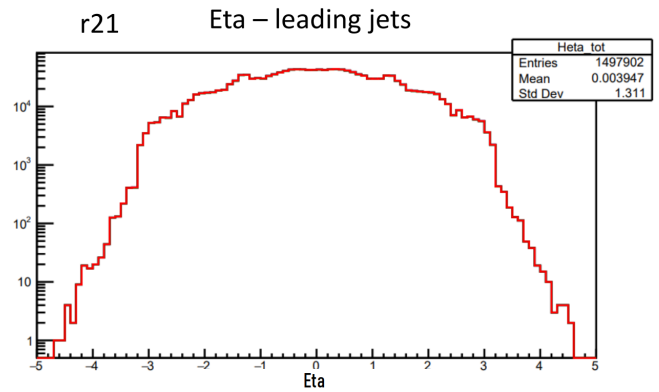


Figure 26: The pseudorapidity, η , distributions of the leading jet sample before and after the respective cuts. Trigger is Hard Probe - r21 release.

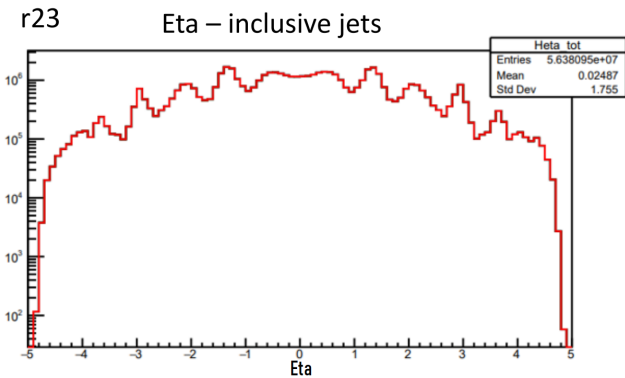


Figure 25: The pseudorapidity, η , distributions of the inclusive jet sample before and after the respective cuts. Trigger is Hard Probe - r23 release.

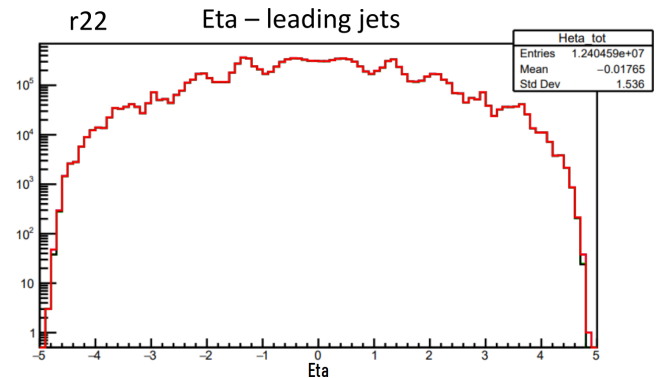


Figure 27: The pseudorapidity, η , distributions of the leading jet sample before and after the respective cuts. Trigger is Hard Probe - r22 release.

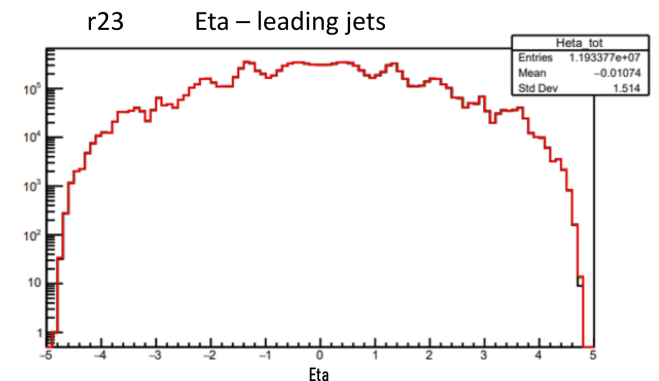


Figure 28: The pseudorapidity, η , distributions of the leading jet sample before and after the respective cuts. Trigger is Hard Probe - r23 release.

It is visible in 24 that the r22 release creates a more homogeneous distribution, without a pronounced central peak. This may be due to a larger acceptance of low p_T jets, as can be seen in 15, where the peak is slightly to the left of other inclusive sets.

Here the 26 graph has a wider border region where the jet number diminishes greatly, starting at $|\eta| \approx 3$, instead of

$|\eta| \approx 4.5$, at r22 or r23 leading sets. This is not visible in sub-leading sets, however.

3.2.6 η graphs - sub-leading set

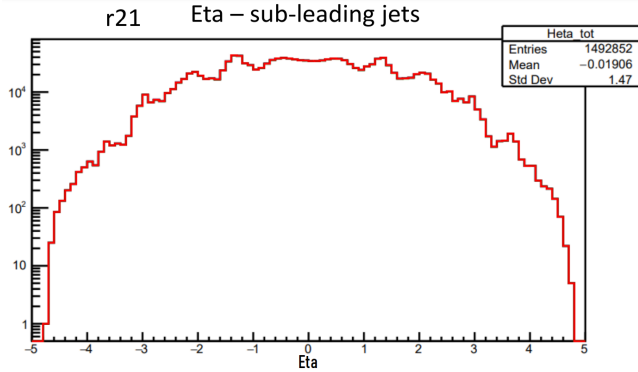


Figure 29: The pseudorapidity, η , distributions of the sub-leading jet sample before and after the respective cuts. Trigger is Hard Probe - r21 release.

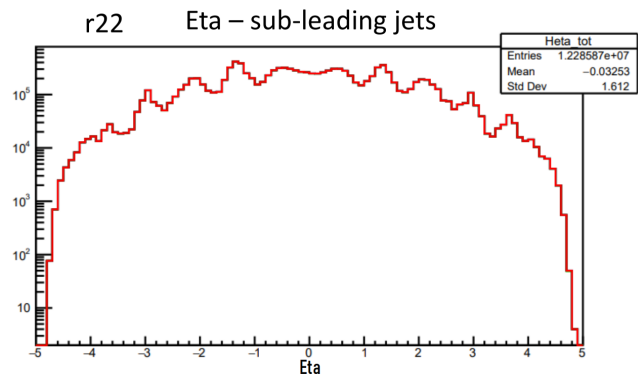


Figure 30: The pseudorapidity, η , distributions of the sub-leading jet sample before and after the respective cuts. Trigger is Hard Probe - r22 release.

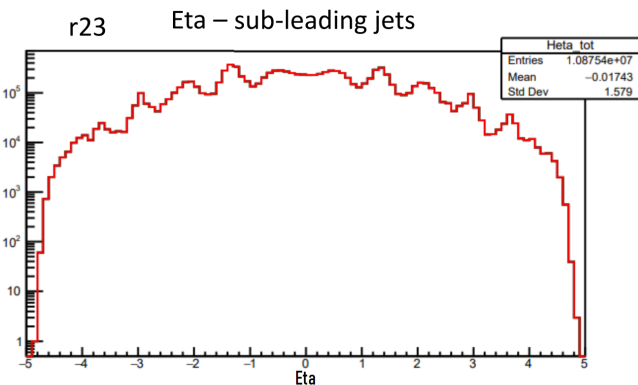


Figure 31: The pseudorapidity, η , distributions of the sub-leading jet sample before and after the respective cuts. Trigger is Hard Probe - r23 release.

4 Data visualization - p_T Cuts

A complete overlap between the 'No Cut' line and 'pt > 10 GeV' cut is observed, showing that only a very small amount of data was cut to remove Electronic Noise.

4.1 Minimum Bias trigger

4.1.1 η graphs

The three software releases were analysed, and will be here presented.

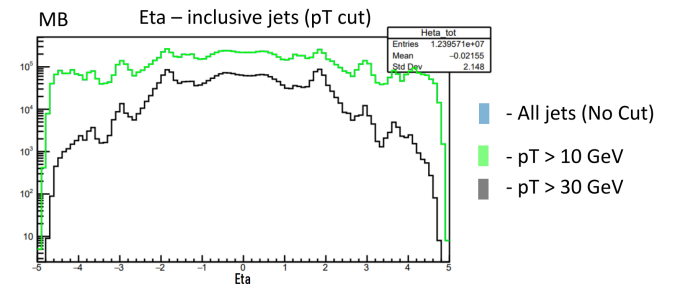


Figure 32: The pseudorapidity, η , distributions of the inclusive jet sample before and after the p_T cuts in legend. Trigger is Minimum Bias.

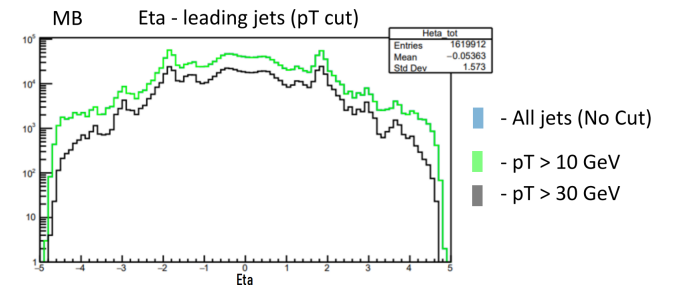


Figure 33: The pseudorapidity, η , distributions of the leading jet sample before and after the p_T cuts in legend. Trigger is Minimum Bias.

It is visible that in the inclusive set the "pT > 30 GeV" cut is quite effective at filtering out results of high $|\eta|$, in comparison to other sets. However, there is a great similarity in this cut between the 3 sets, pointing to close distributions among high-momentum jets.

4.1.2 ϕ graphs

The three software releases were analysed, and will be here presented.

In the inclusive data-set, a greater dampening of the jet peaks is observed in the "pT > 30 GeV" cut, in comparison to the other sets, and in this same data, a spread of the $\phi \approx -1.6$ peak is observed, suggesting this is a high- p_T phenomenon.

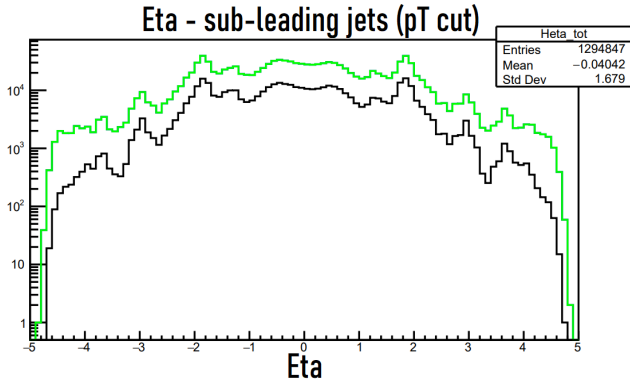


Figure 34: The pseudorapidity, η , distributions of the sub-leading jet sample before and after the p_T cuts in legend. Trigger is Minimum Bias.

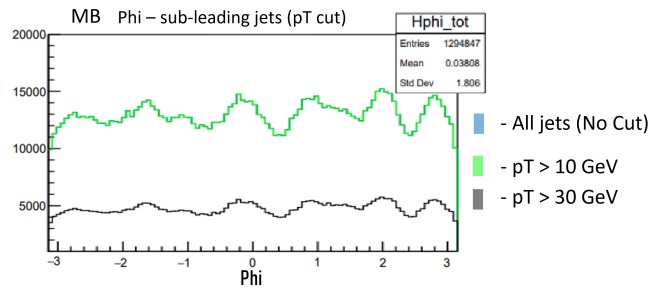


Figure 37: The azimuthal angle, ϕ , distributions of the sub-leading jet sample before and after the p_T cuts in legend. Trigger is Minimum Bias.

4.2 Hard Probes trigger

4.2.1 η graphs - inclusive data-sets

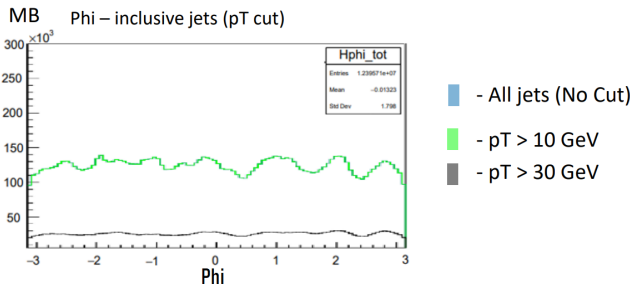


Figure 35: The azimuthal angle, ϕ , distributions of the inclusive jet sample before and after the p_T cuts in legend. Trigger is Minimum Bias.

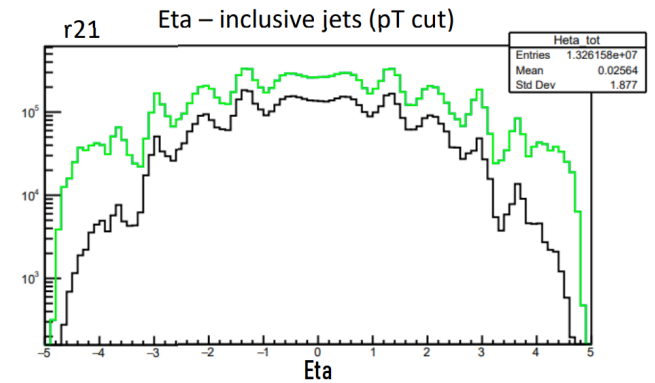


Figure 38: The pseudorapidity, η , distributions of the inclusive jet sample before and after the p_T cuts. Trigger is Hard Probes - r21 release.

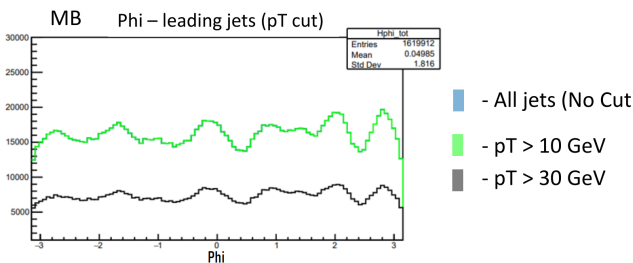


Figure 36: The azimuthal angle, ϕ , distributions of the leading jet sample before and after the p_T cuts in legend. Trigger is Minimum Bias.

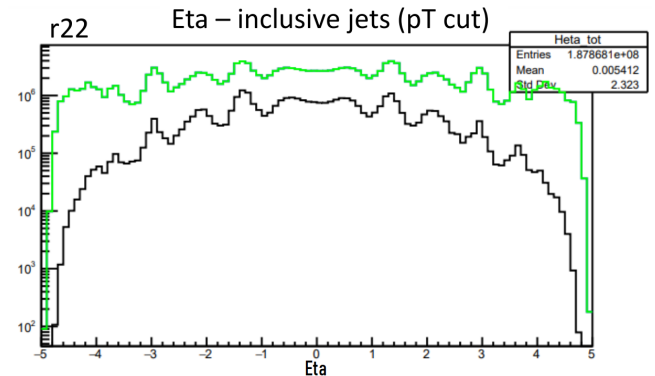


Figure 39: The pseudorapidity, η , distributions of the inclusive jet sample before and after the p_T cuts. Trigger is Hard Probes - r22 release.

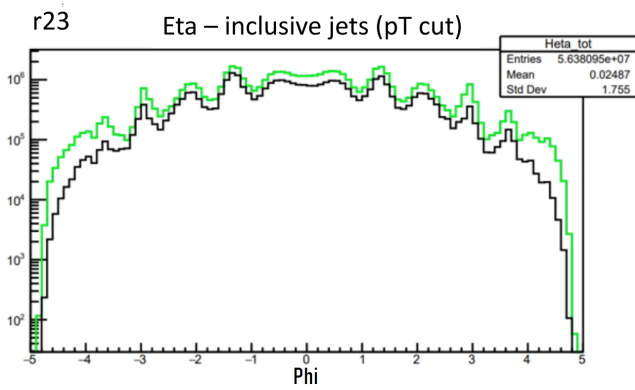


Figure 40: The pseudorapidity, η , distributions of the inclusive jet sample before and after the p_T cuts. Trigger is Hard Probes - r23 release.

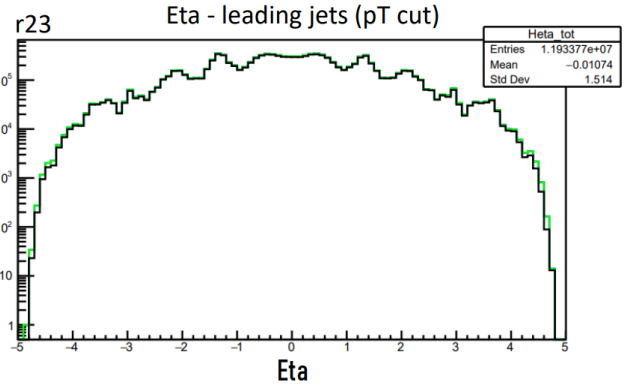


Figure 43: The pseudorapidity, η , distributions of the leading jet sample before and after the p_T cuts. Trigger is Hard Probes - r23 release.

4.2.2 η graphs - leading data-sets

4.2.3 η graphs - sub-leading data-sets

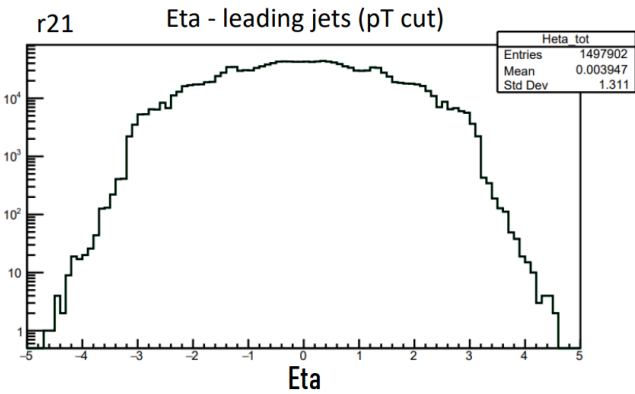


Figure 41: The pseudorapidity, η , distributions of the leading jet sample before and after the p_T cuts. Trigger is Hard Probes - r21 release.

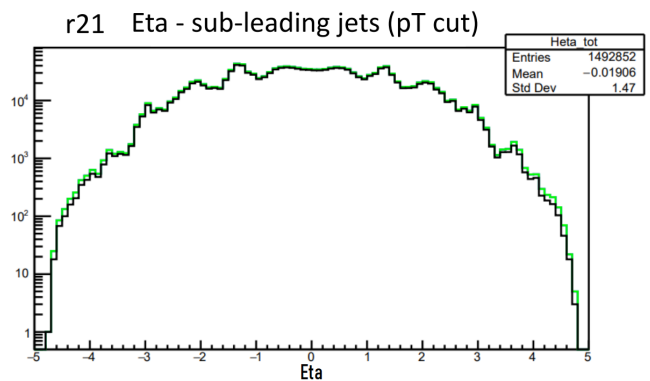


Figure 44: The pseudorapidity, η , distributions of the sub-leading jet sample before and after the p_T cuts. Trigger is Hard Probes - r21 release.

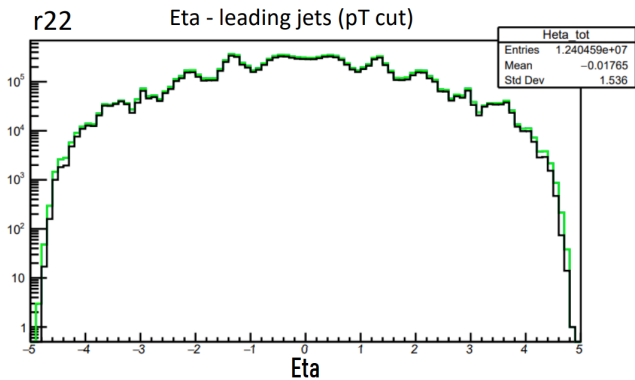


Figure 42: The pseudorapidity, η , distributions of the leading jet sample before and after the p_T cuts. Trigger is Hard Probes - r22 release.

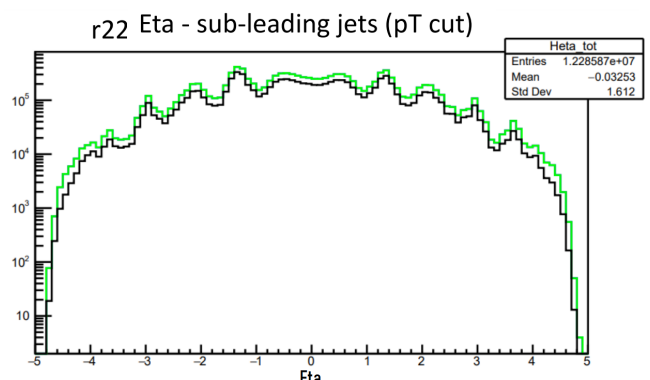


Figure 45: The pseudorapidity, η , distributions of the sub-leading jet sample before and after the p_T cuts. Trigger is Hard Probes - r22 release.

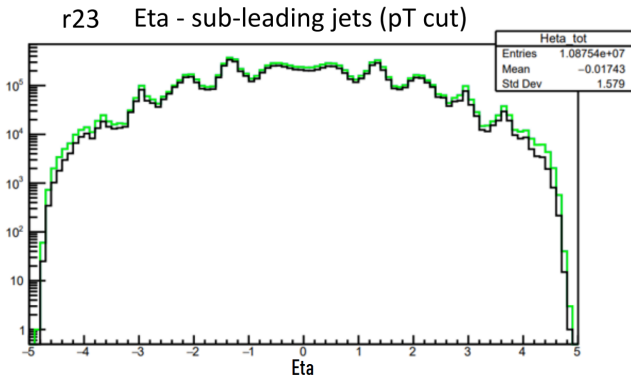


Figure 46: The pseudorapidity, η , distributions of the sub-leading jet sample before and after the p_T cuts. Trigger is Hard Probes - r23 release.

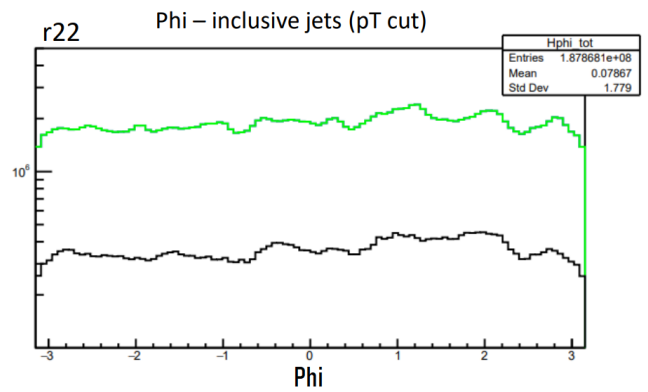


Figure 48: The azimuthal angle, ϕ , distributions of the inclusive jet sample before and after the p_T cuts. Trigger is Hard Probes - r22 release.

The leading sets are hardly affected by the cuts since they are the jets with the highest p_T per event. On the sub-leading sets, the jets most affected are, as expected, those with highest $|\eta|$.

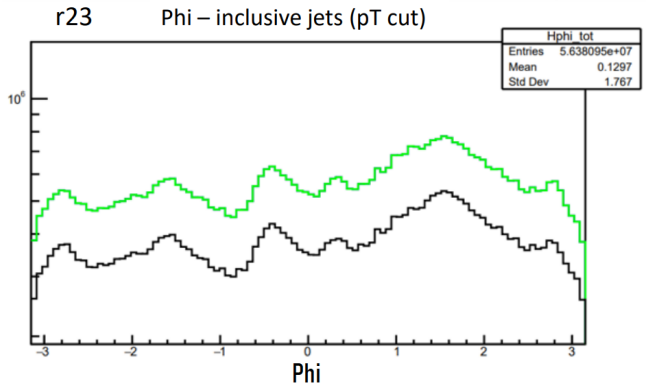


Figure 49: The azimuthal angle, ϕ , distributions of the inclusive jet sample before and after the p_T cuts. Trigger is Hard Probes - r23 release.

4.2.4 ϕ graphs - inclusive data-sets

4.2.5 ϕ graphs - leading data-sets

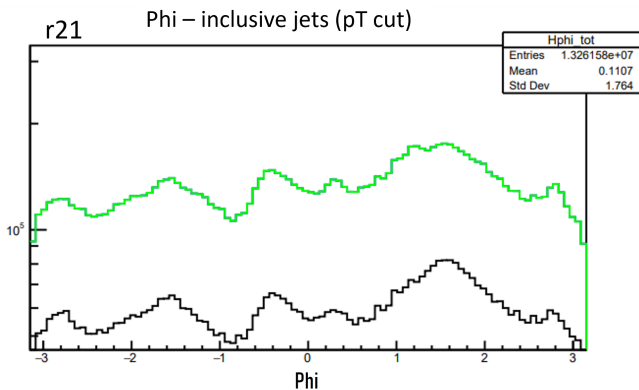


Figure 47: The azimuthal angle, ϕ , distributions of the inclusive jet sample before and after the p_T cuts. Trigger is Hard Probes - r21 release.

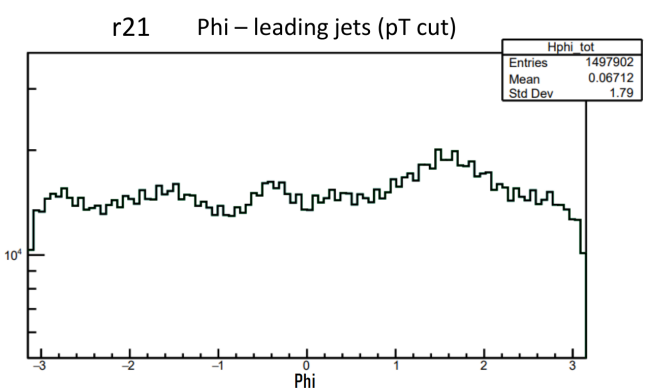


Figure 50: The azimuthal angle, ϕ , distributions of the leading jet sample before and after the p_T cuts. Trigger is Hard Probes - r21 release.

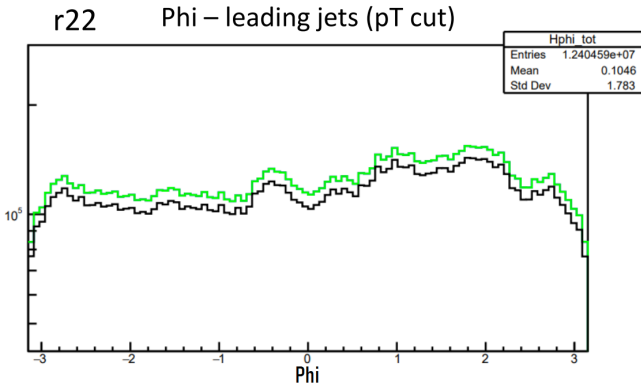


Figure 51: The azimuthal angle, ϕ , distributions of the leading jet sample before and after the p_T cuts. Trigger is Hard Probes - r22 release.

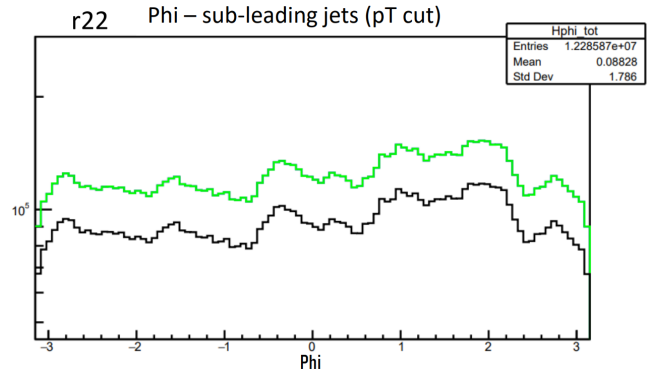


Figure 54: The azimuthal angle, ϕ , distributions of the leading jet sample before and after the p_T cuts. Trigger is Hard Probes - r22 release.

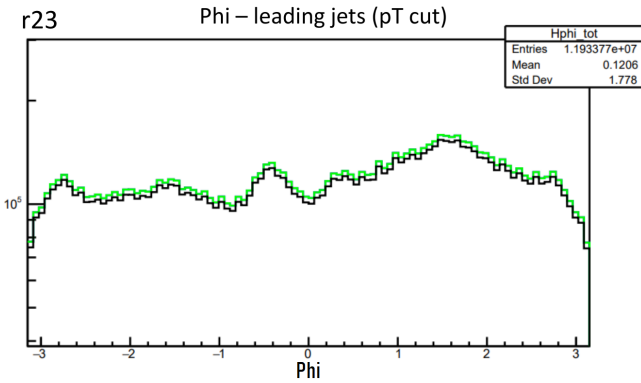


Figure 52: The azimuthal angle, ϕ , distributions of the leading jet sample before and after the p_T cuts. Trigger is Hard Probes - r23 release.

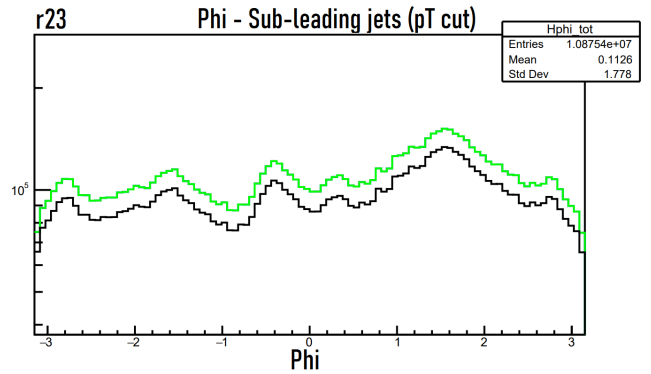


Figure 55: The azimuthal angle, ϕ , distributions of the leading jet sample before and after the p_T cuts. Trigger is Hard Probes - r23 release.

4.2.6 ϕ graphs - sub-leading data-sets

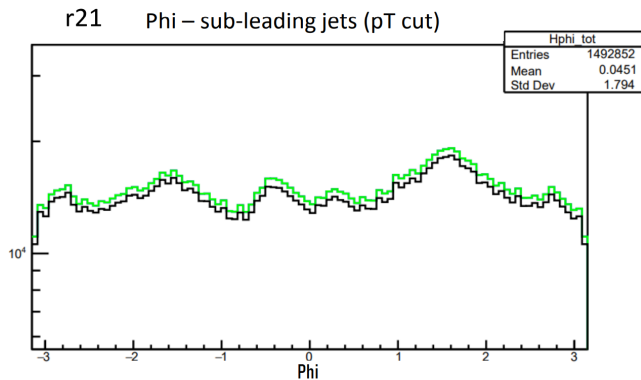


Figure 53: The azimuthal angle, ϕ , distributions of the leading jet sample before and after the p_T cuts. Trigger is Hard Probes - r23 release.

From the sub-leading and leading jets, the r22 data-set was the most affected by the " $p_T > 30$ GeV" cut, and the sub-leading sets are more affected by this cut than the leading, since they have lower p_T values.

Once again we observe that the filter does not change the peak locations, indicating that the angular distribution is not dependent of p_T in this range.

5 Conclusions

In the kinematic variable cuts, it was seen that for Hard Probe data, the " $NPV=1$ " and the " $F_{Cal_Et} > 0.1$ " cuts overlapped.

Besides this, the kinematic variable cuts were much more efficient to filter the Minimum Bias Trigger data than the Hard Probe data, indicating a possible usage in combination with the MB trigger, as can be seen, for example, in the Figure 5, where the " $NPV = 1$ " cut made the p_T distribution similar to those in the Hard Probes Streams. The " $\mu < 1$ " cut has significantly reduced lower p_T jet numbers (from MB) serving perhaps as complementary to the NPV cut.

On the other hand, the " $p_T > 30$ GeV" cut produced significant results in the inclusive HP data-sets, and visible

results in the sub-leading HP data-sets, having negligible effects on the leading HP data-sets.

Acknowledgements

I kindly thank my tutor for the support and availability in answering questions and arranging meetings, and LIP for the internship opportunity, as well as the Pauli machines available for running the code.

References

- [1] ATLAS, *Calorimeter*, <https://atlas.cern/Discover/Detector/Calorimeter> (2023), [Online]
- [2] ATLAS, *Inner detector*, <https://atlas.cern/Discover/Detector/Inner-Detector> (2023), [Online]
- [3] ATLAS, *luminosity*, <https://atlas.cern/Glossary/luminosity> (2023), [Online]
- [4] G.P.Salam, *The European Physical Journal C* (2010)
- [5] L. Cunqueiro, A.M. Sickles, *Progress in Particle and Nuclear Physics* (2022)